(2) 24

NEW MATERIALS FOR INFRARED TRANSMITTING ELECTROOPTIC FILTERS

Quarterly Technical Report No. 4

For period 1 November 1978 through 31 January 1979

Contract MDA 903–78–C–0180

Program Code Number 8D10

Program Element Code 61101E

Hughes Research Laboratories
3011 Malibu Canyon Road
Malibu, CA 90265

Sponsored by

Defense Advanced Research Projects Agency (DoD)

DARPA Order No. 3519

Monitored by DARPA under Contract MDA 903–78–C–0180

A.L. Gentile
Principal Investigator
(213) 456-6411

The views and conclusions contained in this document are those of the authors and should not be interpreted as necessarily representing the official policies, either expressed or implied, of the Defense Advanced Research Projects Agency or the U.S. Government.

ARPA Order Number	3519
Name of Contractor	Hughes Research Laboratories 3011 Malibu Canyon Road Malibu, CA 90265
Effective Date of Contract	1 February 1978
Contract Expiration Date	31 March 1980
Contract Number	MDA 903-78-C-0180
Name and Phone Number of Principal Investigator	A.L. Gentile (213) 456-6411
Contract Period Covered by This Report	1 November 1978 through 31 January 1979

UNCLASSIFIED

SECURITY CLASSIFICATION OF THIS PAGE (When Data Entered)

REPORT DOCUMENTATION PAGE	READ INSTRUCTIONS BEFORE COMPLETING FORM
1. REPORT NUMBER	2. GOVT ACCESSION NO. AD-A139 216 / 3. RECIPIENT'S CATALOG NUMBER
4. TITLE (and Subtitle) NEW MATERIALS FOR INFRARED TRANSMITTING ELECTROOPTIC FILTERS	5. TYPE OF REPORT & PERIOD COVERED Quarterly Tech. Report 4 1 Nov 1978 - 31 Jan 1979
	6. PERFORMING ORG. REPORT NUMBER
7. AUTHOR(s) A.L. Gentile, N.R. Kyle, S.R. Sashital, P.L. Richards, A. Yariv, and C. Shih	8. CONTRACT OR GRANT NUMBER(s) MDA 903-78-C-0180
9. PERFORMING ORGANIZATION NAME AND ADDRESS Hughes Research Laboratories 3011 Malibu Canyon Road Malibu, CA 90265	10. PROGRAM ELEMENT, PROJECT, TASK AREA & WORK UNIT NUMBERS Program Code No. 8D10 Program Element Code 61101E
11. CONTROLLING OFFICE NAME AND ADDRESS Defense Advanced Research Projects Agcy (DoD) 1400 Wilson Boulevard Arlington, VA 22209	12. REPORT DATE March 1979
	13. NUMBER OF PAGES 26
14. MONITORING AGENCY NAME & ADDRESS(if different from Controlling Office)	15. SECURITY CLASS. (of this report) UNCLASSIFIED
	15a. DECLASSIFICATION DOWNGRADING SCHEDULE

16. DISTRIBUTION STATEMENT (of this Report)

Approved for public release; distribution unlimited.

17. DISTRIBUTION STATEMENT (of the abstract entered in Block 20, if different from Report)

18. SUPPLEMENTARY NOTES

19. KEY WORDS (Continue on reverse side if necessary and identify by block number)

Electrooptic materials
IR materials
Binary chalcogenides
Ternary chalcogenides
"Defect" chalcopyrites

20. ABSTRACT (Continue on reverse side if necessary and identify by block number)

The objectives of this program are to find and develop new ~~IR~~ Infrared transmitting materials and to provide new data on the electrooptic (EO) properties of those most likely to have an EO coefficient an order of magnitude higher than materials currently in development for tunable filters. The main technical problems anticipated include the synthesis and single-crystal growth of these materials: many are poorly

DD FORM 1 JAN 73 1473 EDITION OF 1 NOV 65 IS OBSOLETE

UNCLASSIFIED

SECURITY CLASSIFICATION OF THIS PAGE (When Data Entered)

characterized and others have high melting points or melt incongruently. Our approach will overcome these obstacles by first synthesizing approximately 20 polycrystalline samples. Subsequently, their dielectric constants at low and ambient temperatures will be determined, and the two best materials of the survey will be grown as single crystals (second year of the program).

During the last quarter, vapor transport growth of $A^{II}B_2^{III}C_4^{VI}$ chalcogenides using HCl as transport medium continued. Runs involving $ZnGa_2S_4$ and $CdGa_2Se_4$ indicated the need for high temperature and high HCl overpressure for successful transport. Materials evaluation included determination of the dielectric constants for $CuInSe_2$ and $ZnSiAs_2$, which range, respectively, from 36.81 and 34.78 at 6 kHz to 35.71 and 32.91 at 400 kHz. Evaluation resumed after solving contact problems by employing blocking contacts for the capacitance measurement. The mathematics for the capacitance measurements we developed appears in the appendix. The dielectric relaxation spectrum was determined for $ZnSiAs_2$. Far-infrared spectroscopy was performed for $AgInTe_2$ in the region where $\varepsilon = n^2$, and n was determined to equal 3.40.

A theoretical model for the electrooptic effect is described. Calculations based on this model showed excellent agreement with measured values for binary semiconducting compounds.

TABLE OF CONTENTS

REPORT SUMMARY

The objectives of this program are to find and develop new IR transmitting materials and to provide new data on the electrooptic (EO) properties of those most likely to have an EO coefficient an order of magnitude higher than materials currently in development for tunable filters. The main technical problems anticipated include the synthesis and single-crystal growth of these materials: many are poorly characterized and others have high melting points or melt incongruently. Our approach will overcome these obstacles by first synthesizing 20 polycrystalline samples; subsequently, dielectric constants at low and ambient temperatures will be determined and the two best materials of the survey will be grown as single crystals (second year of the program).

During the last quarter, vapor transport growth of $A^{II}B_2^{III}C_4^{VI}$ chalcogenides using HCl as transport medium continued. Runs involving $ZnGa_2S_4$ and $CdGa_2Se_4$ indicated the need for high temperature and high HCl overpressure for successful transport. Materials evaluation included determination of the dielectric constants for $CuInSe_2$ and $ZnSiAs_2$, which range, respectively, from 36.81 and 34.78 at 6 kHz to 35.71 and 32.91 at 400 kHz. Evaluation resumed after a delay caused by contact problems on these materials; the problem was solved by using blocking contacts. The mathematics for the capacitance measurement we developed appear in the appendix. The dielectric relaxation spectrum was determined for $ZnSiAs_2$; peaks corresponded to relaxation times of 16 μsec and 0.7 μsec. Far-infrared spectroscopy was performed for $AgInTe_2$ in the region beyond the Restrahlen, where the dielectric constant $\epsilon = n^2$ (index of refraction), and n was determined to equal 3.40.

A theoretical model for the electrooptic effect in crystals has been developed. Calculations of the electrooptic coefficients based on this model for many binary semiconducting compounds showed excellent agreement with calculated values.

SECTION 1

INTRODUCTION AND SUMMARY

A. PROGRAM OBJECTIVES

The objectives of this program are to find and develop new IR transmitting materials and to provide new data on the electrooptic (EO) properties of those most likely to have EO coefficients an order of magnitude higher than materials currently in development for tunable filters.

The main technical problems anticipated include the synthesis and single-crystal growth of these materials: many are poorly characterized and others have high melting points or melt incongruently. Our approach will overcome these obstacles. First, we will synthesize 20 polycrystalline samples. Then the dielectric constant of each, at both low and ambient temperatures, will be determined, and the two best materials of the survey will be grown as single crystals (second year of the program).

B. SUMMARY

During the last quarter, investigation of vapor transport growth of $A^{II}B_2^{III}C_4^{VI}$ chalcogenides using HCl as a transport medium continued. Runs were made for the reaction and transport of $ZnGa_2S_4$ and $CdGa_2Se_4$. Although complete transport was achieved for $ZnGa_2S_4$, the resulting ingot contained 3 phases, indicating incomplete reaction. Very little transport occurred in the $CdGa_2Se_4$ run. Indications are that high temperature (>1000°C) as well as elevated HCl pressures (2 to 3 atm at operating conditions) are required for successful transport and complete reaction of these materials.

The determination of dielectric constants for previously synthesized samples has been impeded by contact problems. Metallic contacts consisting of constituent elemental metals have yielded Schottky barriers, as well as filamentary shorts caused by metal transport via pores

and grain boundaries in these polycrystalline samples. We have developed a method for measuring the capacitance in which blocking contacts are used; the mathematical calculation is presented in the appendix. Recent results using this technique indicated dielectric constants ranging from 36.81 (6 kHz) to 35.71 (400 kHz) for $CuInSe_2$, and 34.78 (6 kHz) to 32.91 (400 kHz) for $ZnSiAs_2$. These results show dielectric constants approximately three times greater than those observed in our previous measurements for GeS_2 and $AgGaS_2$. The dielectric relaxation spectrum for $ZnSiAs_2$ showed peaks corresponding to relaxation times of 16 μsec and 0.7 μsec. The index of refraction for $AgInTe_2$ was measured in the far infrared (beyond Restrahlen), where the dielectric constant $\varepsilon = n^2$, and found to be 3.40, yielding $\varepsilon = 11.6$.

A theoretical model for the EO effect in crystals has been developed. Predicted EO coefficients based on this model for binary semiconductor compounds are in excellent agreement with measured values. We plan to extend the model to the ternary chalcogenide crystals and eventually to compare predicted results with measurements achieved on this program.

SECTION 2

MATERIALS PREPARATION AND CRYSTAL GROWTH: VAPOR TRANSPORT OF TERNARY CHALCOGENIDES

Early observations of little or no transport using iodine as the carrier gas for the vapor transport growth of ternary chalcogenides of the type $A^{II}B_2^{III}C_4^{VI}$ led to the use of HCl, which was reported to be a more effective carrier. In our third quarterly report, several initial attempts at growth using HCl were discussed. To summarize, using HCl had improved the quantity of transported material compared with iodine, and some materials (e.g., $CdIn_2S_4$, and $CdIn_2Se_4$) had been obtained in sufficient quantities to prepare samples for evaluation. During the fourth quarter, we attempted to synthesize $ZnGa_2S_4$ using HCl as the transport medium.

In the case of $ZnGa_2S_4$, all starting material was transported to the conical end of the sealed ampoule at temperatures as high as 1100°C. The ampoule contained three distinct bands: yellow, white, and translucent. The sample of $CdGa_2Se_4$ showed almost no transport, yielding only a thin coating showing two different colors. The temperature in the hot zone was ∿900°C; 1 atm of HCl was maintained at the operating temperature.

Results indicate the need for increased temperature (1000°C appears useful) and increased pressure of HCl at operating temperatures. A review of recent crystal growth literature has uncovered a report of the use of 2 to 3 atm pressure of HCl under operating conditions for a successful yield of ternary chalcogenide compounds by vapor transport to crystal growth.

Our next series of runs will incorporate the above conditions (i.e., high temperature and higher (2 to 3 atm) pressure of HCl) for growth of $A^{II}B_2^{III}C_4^{IV}$ compounds.

SECTION 3

MATERIALS EVALUATION

A. DIELECTRIC CONSTANT MEASUREMENTS

The ability to make accurate capacitance and dielectric relaxation measurements on a new insulating or semi-insulating compound depends markedly on the availability of a good metalization system for electrical contacts. If high Schottky barriers are formed at the metal-contact/insulator interface and the insulator does not have a sufficiently high resistance (10^7 Ω or higher), the measured capacitance will be rather high and essentially will represent the Schottky-barrier capacitance. As described in the last quarterly report, this phenomenon was observed with $ZnSiAs_2$ having silver paint electrodes. An absurdly high value (ϵ = 9500) was measured for the dielectric constant. The fact that this was genuinely a Schottky-barrier effect was ascertained by applying a voltage bias to the capacitor and observing the change of capacitance. Although it is true that, for any given material, a metal or an alloy system may be found to yield non-barrier-forming contacts, the search for such contacts for the new materials made for this program would be a major undertaking. Alternatively, if a suitable metal, which is also a constituent of the ternary chalcogenide (e.g., In for $CdIn_2Se_4$, $CuInSe_2$, and $AgInSe_2$), is used as the contact and further diffused into the shallow surface layers of the chalcogenide, a graded, nearly Ohmic junction may be expected at the metal-insulator interface. Although this approach has worked well with single crystals (e.g., Ag on $AgGaS_2$), it has one main drawback with polycrystalline insulators. Even after a moderate diffusion anneal of In in polycrystalline $CuInSe_2$, $AgInSe_2$, and $CdIn_2Se_4$, we observed that the samples were essentially shorted or exhibited resistances on the order of a few hundred ohms and therefore could not be measured. We believe that the shorts are caused

by diffusion of the metal along grain boundaries and the subsequent formation of conducting filaments across the bulk of the insulator.

As a solution to these problems, we decided that capacitance measurements should be made with two blocking contacts. This also prevents carrier injection. The blocking electrodes consist of two thin (0.004 in.) sheets of Mylar with evaporated silver contacts. The Mylar capacitors have the same area as the test insulator. The insulator is sandwiched between the two Mylar capacitors, and the capacitance C_m and the equivalent parallel resistance R_m of the sandwich structure at a frequency ω are measured using a Boonton 750C capacitance bridge. The insulator is then removed from the sandwich, and the total capacitance C_s and shunt resistance R_s are measured at the same frequency ω. A network analysis of the equivalent circuits for the two cases yields the capacitance C_t and resistance R_t of the test insulator (as shown in the appendix).

The dielectric constants of $CuInSe_2$ and $ZnSiAs_2$ measured at room temperature according to the above procedure at several frequencies in the range of 6 to 400 kHz are shown below in Table 1.

Table 1. Dielectric Constant Values at Indicated Frequencies

Frequency	6 kHz	10 kHz	100 kHz	400 kHz
$CuInSe_2$	36.81	36.15	35.74	35.71
$ZnSiAs_2$	34.78	34.65	33.64	32.91

B. DIELECTRIC RELAXATION

The dielectric relaxation spectrum, a plot of the dissipation factor (tan δ) versus frequency for $ZnSiAs_2$, is shown in Figure 1. There are two distinct peaks corresponding to frequencies of 60 kHz and 220 kHz, which correspond to relaxation times of 16 μsec and 0.7 μsec, respectively. Although sufficient details of the defect structure of this sample are not presently available to draw any definite conclusions, we can speculate that the shorter time constant, 0.7 μsec, corresponds to the jump frequency of the lightest of host ions, silicon, into and out of Si vacancies. The longer time constant of 16 μsec may be due to similar jump frequencies of the other host cation, zinc. The host anion, arsenic, because of its large mass, is not expected to respond to the applied high frequency of electric fields corresponding to the observed peaks. Similar and more detailed studies are in progress on other materials grown on this program.

C. FAR-INFRARED SPECTROSCOPY

The far-infrared transmission spectrum of $AgInTe_2$ (Figure 2) was determined and analyzed under the direction of Professor Paul L. Richards (Department of Physics, University of California at Berkeley). Sample thickness was measured to be 0.113 cm. The index of refraction was determined to be 3.40, and no noticeable dispersion over the measured frequency range was observed.

D. A THEORETICAL MODEL FOR THE ELECTROOPTIC EFFECT IN CRYSTALS

In this section, we develop a theoretical model* for the EO effect. The main motivation is to obtain an expression that can be used to predict the EO coefficient of new crystals. The data needed in the

*Model developed by A. Yariv and C. Shih.

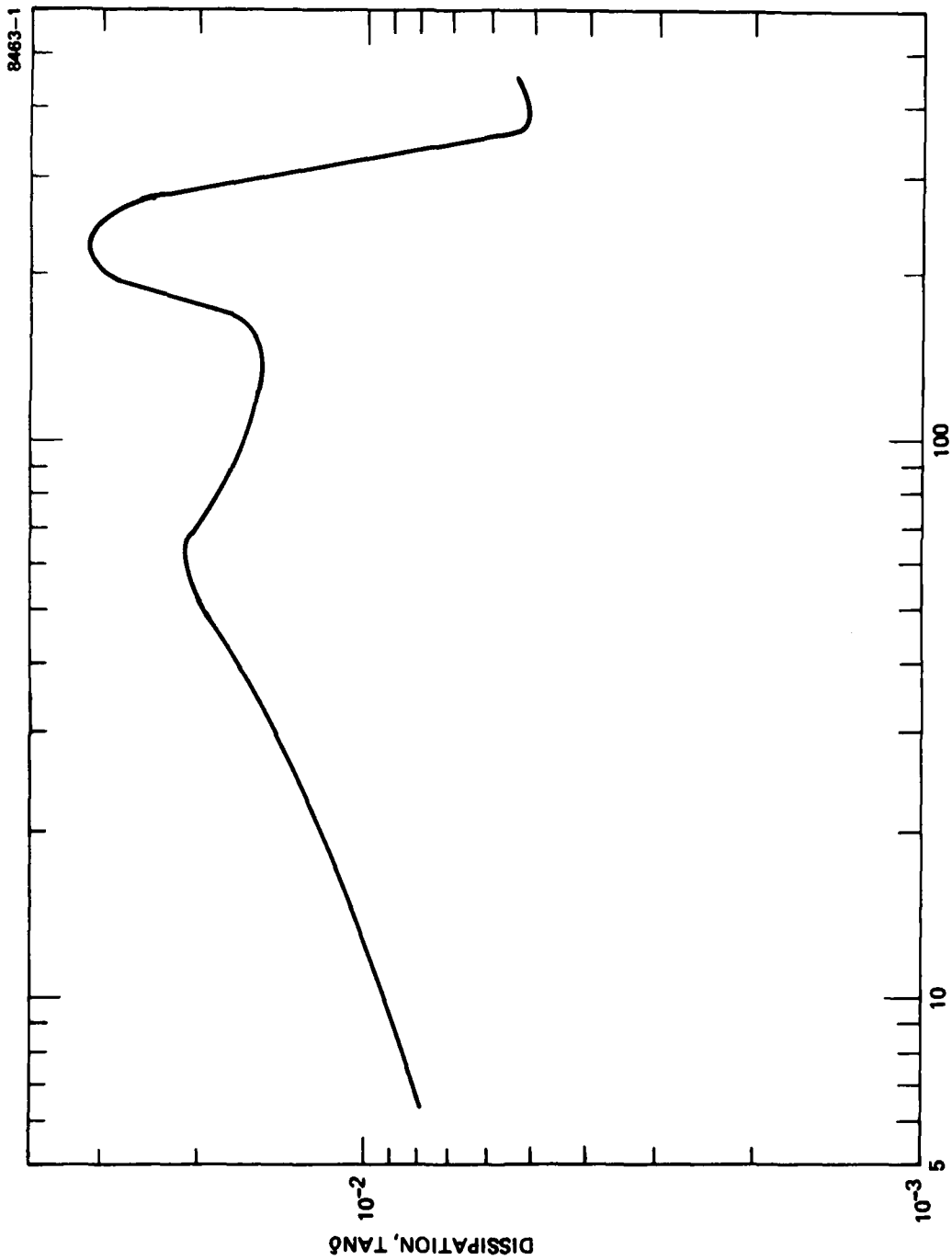

Figure 1. Dielectric relaxation of $ZnSiAs_2$

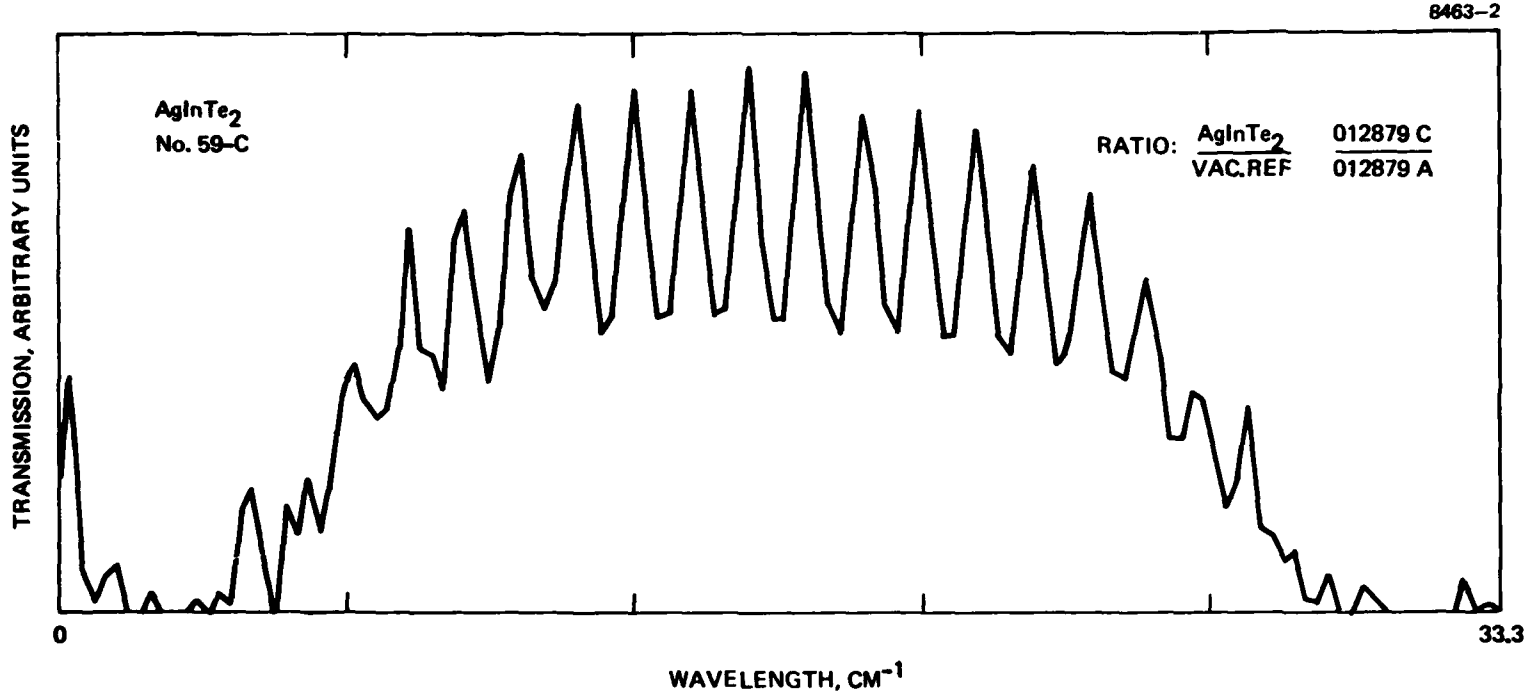

Figure 2. Far-IR transmission of $AgInTe_2$.

evaluation of the EO coefficients consist of "low"-frequency* and optical-frequency dielectric constants, crystal structure (symmetry class and dimensions), bond ionicity, and ionic charges. These data are available and tabulated for a large number of crystals, including many for which the EO coefficient has not yet been measured. The nonlinear optical constants of the crystal can be used, when available, to simplify the numerical determination of the EO coefficients.

The EO effect consists of a change in the optical properties of crystals caused by an applied dc or "low"-frequency electric field.

The EO effect in a crystal is specified by giving the elements r_{ijk} of the EO tensor. This tensor relates the change of the relative dielectric tensor $\varepsilon'_{ij} = \varepsilon_{ij}/\varepsilon_o$ to the applied low-frequency field E^{Ω}_{k} via the relation[1]

$$\Delta\varepsilon'_{ij} = \Delta\chi_{ij} = -\varepsilon'_{ii}\varepsilon'_{jj} r_{ijk} E^{\Omega}_{k} \quad , \tag{1}$$

where χ_{ij} are the elements of the susceptibility tensor, which relates the induced optical polarization $p^{(\omega)}_{i}$ to the optical field $E^{(\omega)}_{j}$ by

$$p^{\omega}_{i} = \varepsilon_o \chi_{ij} E^{(\omega)}_{j} \quad .$$

In the above equations and in the rest of the analysis, MKS units are used. The superscripts ω and Ω denote optical and low frequencies, respectively. The subscripts specify the Cartesian component. Summation over repeated Cartesian indices is understood.

There are two distinct physical contributions to the EO effect; to distinguish them, refer to Figure 3, which shows a zincblende crystal lattice.

---

*By "low" we mean frequencies below the lattice absorption band, which typically can extend up to 10^{12} to 10^{13} Hz.

evaluation of the EO coefficients consist of "low"-frequency* and optical-frequency dielectric constants, crystal structure (symmetry class and dimensions), bond ionicity, and ionic charges. These data are available and tabulated for a large number of crystals, including many for which the EO coefficient has not yet been measured. The nonlinear optical constants of the crystal can be used, when available, to simplify the numerical determination of the EO coefficients.

The EO effect consists of a change in the optical properties of crystals caused by an applied dc or "low"-frequency electric field.

The EO effect in a crystal is specified by giving the elements r_{ijk} of the EO tensor. This tensor relates the change of the relative dielectric tensor $\varepsilon'_{ij} = \varepsilon_{ij}/\varepsilon_o$ to the applied low-frequency field E^{Ω}_{k} via the relation[1]

$$\Delta\varepsilon'_{ij} = \Delta\chi_{ij} = -\varepsilon'_{ii}\varepsilon'_{jj} r_{ijk} E^{\Omega}_{k} \quad , \tag{1}$$

where χ_{ij} are the elements of the susceptibility tensor, which relates the induced optical polarization p^{ω}_{i} to the optical field E_j by

$$p^{\omega}_{i} = \varepsilon_o \chi_{ij} E^{\omega}_{j} \quad .$$

In the above equations and in the rest of the analysis, MKS units are used. The superscripts ω and Ω denote optical and low frequencies, respectively. The subscripts specify the Cartesian component. Summation over repeated Cartesian indices is understood.

There are two distinct physical contributions to the EO effect; to distinguish them, refer to Figure 3, which shows a zincblende crystal lattice.

---

*By "low" we mean frequencies below the lattice absorption band, which typically can extend up to 10^{12} to 10^{13} Hz.

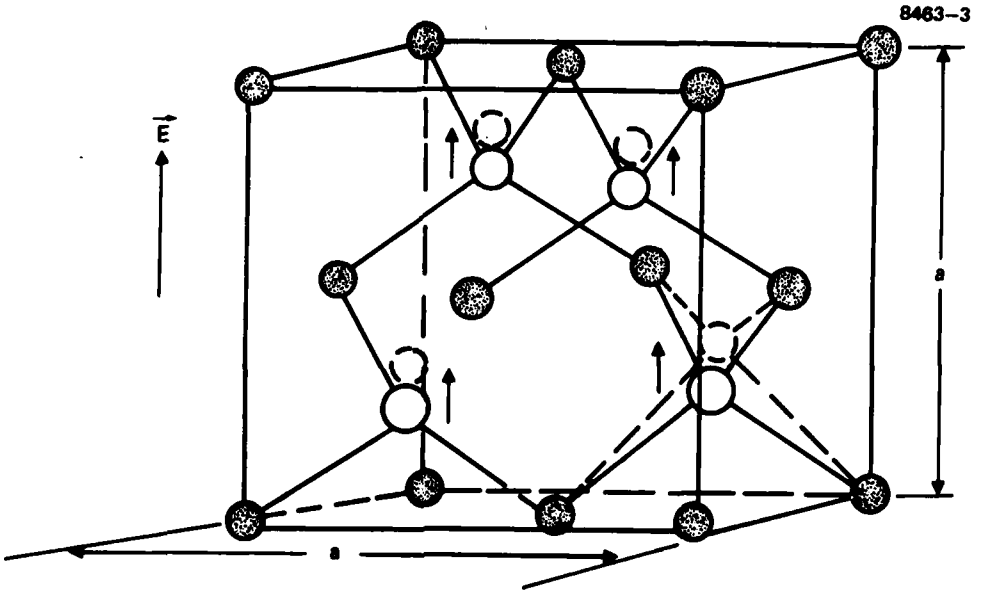

Figure 3. Zincblende crystal lattice.

The first contribution results from a rearrangement of the electron distribution alone and does not involve a motion of the atoms. The contribution of this mechanism to the EO tensor — $(r_{ijk})_{elec}$ — is related to the coefficient of second harmonic generation $d_{ijk}^{2\omega = \omega+\omega}$ by

$$(r_{ijk})_{elec} = -\frac{4\varepsilon_o}{\varepsilon_j \varepsilon_i} d_{ikj}^{2\omega = \omega+\omega} \quad . \tag{2}$$

A theoretical model developed by Levine[2] and based on the Phillips-Van Vechten[3] (P-VV) dielectric theory[1] has been quite successful in calculating $(r_{ijk})_{elec}$ using dielectric and ionicity data.

The second contribution to the EO effect is due to the changes in the atomic positions induced by the low-frequency field. This ionic contribution $(r_{ijk})_{ion}$ is the concern of this report. The total EO coefficient is then given by

$$r_{ijk} = (r_{ijk})_{elec} + (r_{ijk})_{ion} \quad . \tag{3}$$

To appreciate qualitatively the nature of the ionic contribution, consider Figure 3. We assume, as does Levine,[2] that the internally induced dipole moments point principally along the bond directions.

Let us consider a single bond, say bond μ, in a unit cell. An optical field E^{ω} along the bond direction will induce a dipole moment

$$p^{\mu} = \chi^{\mu} E^{\omega}$$

along the bond direction. (The dipole components induced normal to the bond are usually at least an order of magnitude less than those induced along the bond.) χ^{μ} is the bond polarizability. If a field E_j^{ω} is

applied, then the component of this field along μ is $E_j^\omega \alpha_j^\mu$, where α_j^μ is the cosine of the angle between the j axis and the direction of bond μ. The induced dipole along μ is then

$$p^\mu = \varepsilon_o \chi^\mu \alpha_j^\mu E_j^\omega \quad .$$

The projection of this dipole along the Cartesian direction i is thus

$$p_i^\mu = \varepsilon_o \chi^\mu \alpha_j^\mu \alpha_i^\mu E_j^\omega \quad .$$

To find the induced polarization (dipole moment per unit volume) along i due to E_j^ω, we must add the contributions due to all the bonds within a unit cell and divide the result by the unit cell volume V:

$$p_i^\omega = \frac{1}{V} \sum_{\substack{\text{bonds} \\ \mu}} \varepsilon_o \chi^\mu \alpha_j^\mu \alpha_i^\mu E_j^\omega$$

$$= \varepsilon_o \chi_{ij} E_j^\omega \quad ,$$

where χ_{ij} is the conventionally defined optical susceptibility tensor. It follows that

$$\chi_{ij} = \frac{1}{V} \sum_{\substack{\text{bonds} \\ \mu}} \chi^\mu \alpha_i^\mu \alpha_j^\mu \quad . \tag{4}$$

The effect of an applied low-frequency electric field, E_k, is to displace the atoms in the lattice as shown. This displacement causes a change in the individual bond lengths and a rotation of the bond axes. The first effect (bond length) modified the bond polarizability, χ^μ; the rotation changes the direction cosine α_j^μ. This, according to Eq. 4, causes χ_{ij} to change.

These effects can be described by taking the differential of Eq. 4:

$$\Delta\chi_{ij} = \frac{1}{V} \sum_{\mu} \left(\Delta\chi^{\mu} \alpha_i^{\mu} \alpha_j^{\mu} + \chi^{\mu} \alpha_i^{\mu} \Delta\alpha_j^{\mu} + \chi^{\mu} \alpha_j^{\mu} \Delta\alpha_i^{\mu} \right) \quad . \tag{5}$$

The first term on the right side of Eq. 5 describes the change in χ_{ij} due to the change in bond length; the last two terms give the rotational effect. To obtain the EO effect from Eq. 5, we need to relate the changes $\Delta\chi^{\mu}$ and $\Delta\alpha_j^{\mu}$ to the applied field E_k. The applied field causes the bond coordinate X_k to change. This change is usually manifested as an induced dipole moment. It follows that

$$Ne_c^* \Delta X_k = \epsilon_o (\epsilon'_{dck} - \epsilon'_{\infty k}) E_k \quad , \tag{6}$$

where N is the number of atom pairs (bonds) per unit volume, and e_c^* is the Callen[4] effective ionic charge. The EO tensor r_{ijk} is then obtained by expressing $\Delta\chi^{\mu}$ and $\Delta\alpha_i^{\mu}$, from Eq. 5, in terms of E_k.

The changes in direction cosines (α_i^{μ}) due to ΔX_k are

$$\Delta\alpha_i^{\mu} = \left(\delta_{ik} - \alpha_i^{\mu} \alpha_k^{\mu} \frac{\Delta X_k}{d_o} \right) , \tag{7}$$

where d_o is the bond length. The change $\Delta\chi^{\mu}$ in the bond polarizability is obtained straightforwardly from the P-VV theory. The final result is

$$(r_{ijk})_{ionic} = - \frac{\epsilon_o (\epsilon'_{dck} - \epsilon'_{\infty k})}{V Ne_c^* \epsilon_{ii} \epsilon_{jj}} \sum_{\mu} \frac{\partial\chi^{\mu}}{d_o} \left[\left(f_i \alpha_i^{\mu} \alpha_j^{\mu} \alpha_k^{\mu} \right) + 1/2 \left(\alpha_i^{\mu} \delta_{jk} + \alpha_j^{\mu} \delta_{ik} \right) \right] , \tag{8}$$

where f_i is the ionicity factor. The ionicity factor can be expressed in terms of bond parameters, which are also used in dielectric theory,[3] and is tabulated in Table 2 for several crystals of the type $A^{II}B^{VI}$ or

$A^{III}B^{V}$. A full derivation for the above equations will be provided in the final report for this program.

The values of f have magnitudes that are all small compared to unity. It follows directly from Eq. 8 that, when the purely geometrical factor

$$\sum_{\mu} \alpha_i^{\mu} \neq 0 \quad , \tag{9}$$

the contribution of the second term,

$$\sum_{\mu} 1/2 \ (\alpha_i^{\mu} \ \delta_{jk} + \alpha_j^{\mu} \ \delta_{ik}) \quad , \tag{10}$$

dominates and is an order of magnitude or so larger than the first term,

$$\sum_{\mu} f_i \alpha_i^{\mu} \ \alpha_j^{\mu} \ \alpha_k^{\mu} \quad . \tag{11}$$

Table 2 summarizes the result of applying the above theory to a number of AB crystals belonging to the zincblende and wurtzite classes. The electronic contribution is obtained from the measure of optical second harmonic generation coefficients d_{ikj} using the relation

$$d_{ikj}^{2\omega=\omega+\omega} = - \frac{\varepsilon_{ii}\varepsilon_{jj}}{4\varepsilon_o} \ r_{ijk} \quad . \tag{12}$$

In the wurtzite structure (e.g., ZnS, $\sum_{\mu} \alpha_i^{\mu} = 0$ for i = 1,2,3), the resulting r_{ion} is small and is comparable but opposite in sign to r_{elec}. The result is that $r_{sum} = r_{elec} + r_{ion}$ is also small. The excellent agreement between the experimentally measured values of r and our calculated values lends support to the validity of this model. (A part of this work was sponsored by the Hughes Aircraft Company).

Table 2. Comparison of Predicted and Measured Values of EO Coefficient for Some Binary Compounds

AB	a_o, a_{eff}	ε_{dc}	ω	f_i	$-f$	$\frac{e_c^*}{e}$	r_{14} or r_{33}, 10^{-12} $\frac{m}{V}$			
							r_{ion}	$-r_{elec}$	$r_{pred.}$	$r_{meas.}$
GaAs	5.65	13.2	0.176	0.310	0.091	0.20	0.94	2.73	-1.8	-1.6
GaP	5.45	12.0	0.284	0.370	0.113	0.23	1.53	3.20	-1.7	-1.1
ZnSe	5.67	9.1	0.433	0.630	0.163	0.33	2.54	4.68	-2.1	2.0[a]
ZnS	5.41	8.3	0.492	0.623	0.179	0.35	2.71	4.77	-2.1	2.1[a]
CuCl	5.41	7.5	0.749	0.749	0.212	0.27	6.35	2.66	+3.7	+3.6
ZnTe	6.09	10.1	0.331	0.546	0.119	0.26	2.07	6.41	+1.7	4.[a]
ZnO	4.57	8.2	0.810	0.616	0.239	0.48	3.58	1.91	-4.3	+1.9
ZnS	5.39	8.7	0.552	0.623	0.181	0.35	3.54	5.63	-2.0	1.8[a]
CdS	5.85	9.4	0.652	0.683	0.162	0.41	3.75	6.71	-3.0	3.0[a]
CdSe	6.08	10.2	0.562	0.699	0.147	0.36	3.61	7.40	-3.8	4.3[a]

[a] Sign not measured.

6326

In the next report, we will describe the application of this method to $LiNbO_3$, $LiTaO_3$, and other crystal classes. The ultimate aim is to select new crystals with high EO coefficients from among IR transmitting chalocogenide crystals.

REFERENCES

1. A. Yariv, "Quantum Electronics" 2nd edition. J. Wiley and Sons pp. 355 and 408 (1967).

2. B.F. Levine, Phys. Rev. Lett 22, 787 (1969), 25, 440 (1970).

3. J.C. Phillips Phys. Rev. Lett. 20, 550, (1968). J.A. Van Vechten, Phys. Rev. 182, 891, (1969), 187, 1007 (1969).

4. H.B. Callen, Phys. Rev. 76, 1394 (1949).

APPENDIX

ANALYSIS OF CAPACITANCE MEASUREMENTS USING BLOCKING CONTACTS

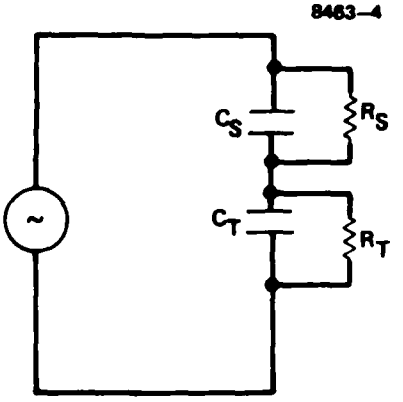

Problem:

An impedance bridge measures the total capacitance C_M and the total resistance (equivalent shunt) R_M of the two capacitors C_S and C_T in series at a frequency f. The bridge independently also measures C_S and R_S. Find the value of C_T and R_T.

Solution:

Since C_S and R_S are in parallel, the net (total) impedance Z_S of C_S and R_S is given by

$$\frac{1}{Z_S} = \left\{ \frac{1}{R_S} + \frac{C_S\omega}{j} \right\},$$

where $\omega = 2\pi f$, and $j = \sqrt{-1}$. Therefore, it follows that

$$Z_S = \frac{R_S}{(1 + \omega^2 R_S^2 C_S^2)} + j \frac{R_S^2 C_S\omega}{(1 + \omega^2 R_S^2 C_S^2)} .$$

Similarly for the circuit of C_T and R_T,

$$Z_T = \frac{R_T}{1 + \omega^2 R_T^2 C_T^2} + j \frac{R_T^2 C_T\omega}{1 + \omega^2 R_T^2 C_T^2} .$$

Since Z_S and Z_T are in series, the total measured Z_M is equal to $Z_S + Z_T$. The measurement of Z_M yields a value for R_M and C_M since

$$Z_M = \left\{ \frac{1}{R_M} + \frac{C_M\omega}{j} \right\}^{-1}$$

$$= \frac{R_M^2}{1+\omega^2 R_M^2 C_M^2} + j \frac{R_M^2 C_M \omega}{1+\omega^2 R_M^2 C_M^2}$$

From $Z_M = Z_S + Z_T$, we get, after equating real and imaginary parts,

$$\frac{R_M}{1 + \omega^2 R_M^2 C_M^2} = \frac{R_S}{1+\omega^2 R_S^2 C_S^2} + \frac{R_T}{1+\omega^2 R_T^2 C_T^2} \qquad \text{(A-1)}$$

and

$$\frac{R_M^2 C_M}{1+\omega^2 R_M^2 C_M^2} = \frac{R_S^2 C_S}{1+\omega^2 R_S^2 C_S^2} + \frac{R_T^2 C_T}{1+\omega^2 R_T^2 C_T^2} \; . \qquad \text{(A-2)}$$

Therefore,

$$\frac{R_T}{1+\omega^2 R_T^2 C_T^2} = \frac{R_M}{1+\omega^2 R_M^2 C_M^2} - \frac{R_S}{1+\omega^2 R_S^2 C_S^2} = \theta, \text{ a constant,}$$

since R_M, R_S, C_M, C_S, and ω are measured values. Then it follows that

$$R_T = \theta + \omega^2 R_T^2 C_T^2 \theta \; .$$

Similarly, from Eq. A-2 we get

$$\frac{R_T^2 C_T}{1+\omega^2 R_T^2 C_T^2} = \frac{R_M^2 C_M}{1+\omega^2 R_M^2 C_M^2} - \frac{R_S^2 C_S}{1+\omega^2 R_S^2 C_S^2} = \lambda, \text{ a constant} \qquad \text{(A-3)}$$

and

$$R_T^2 C_T = \lambda + \lambda\omega^2 R_T^2 C_T^2 \quad . \tag{A-4}$$

Thus, for the two unknowns C_T and R_T, we have two equations:

$$R_T^2 C_T^2 \omega^2 \theta - R_T + \theta = 0 \tag{A-5}$$

and

$$R_T^2 C_T - \lambda - \lambda\omega^2 R_T^2 C_T^2 = 0 \quad . \tag{A-6}$$

The simplest solution will be derived from Eq. A-5:

$$C_T^2 = \frac{R_T - \theta}{R_T^2 \omega^2 \theta}$$

or

$$C_T = \pm\sqrt{\frac{R_T - \theta}{R_T^2 \omega^2 \theta}} \quad .$$

Since only positive roots are possible, we can write

$$C_T = \frac{1}{R_T \omega}\sqrt{\frac{R_T - \theta}{\theta}} \quad .$$

Substituting for C_T^2 in Eq. A-5, after squaring both sides of Eq. A-6, yields

$$R_T^4 C_T^2 = \lambda^2 + 2\lambda^2 \omega^2 R_T^2 C_T^2 + \lambda^2 \omega^4 R_T^4 C_T^4 \quad .$$

From this we obtain

$$R_T^4 = \frac{(R_T-\theta)}{R_T^2 \theta^2} = \lambda^2 + 2\lambda^2 \omega^2 \frac{R_T^2 (R_T-\theta)}{R_T^2 \omega^2 \theta} + \frac{\lambda^2 \omega^4 R_T^4 (R_T-\theta)^2}{R_T^4 \omega^4 \theta^2}$$

or

$$R_T^2 \frac{(R_T-\theta)}{\omega^2 \theta} = \lambda^2 + \frac{2\lambda^2}{\theta} (R_T-\theta) + \frac{\lambda^2 (R_T-\theta)^2}{\theta^2} \quad ,$$

$$\theta R_T^2 (R_T-\theta) = \lambda^2 \omega^2 \theta^2 + 2\lambda^2 \omega^2 \theta (R_T-\theta) + \lambda^2 \omega^2 (R_T-\theta)^2$$

or

$$\lambda^2 \omega^2 R_T^2 - 2\lambda^2 R_T \theta + \lambda^2 \theta^2 + 2\lambda^2 \theta R_T - 2\lambda^2 \theta^2 + \lambda^2 \theta^2 = R_T^3 \theta - R_T^2 \theta^2 \quad .$$

Therefore,

$$R_T^3 \theta - R_T^2 \theta^2 = \lambda^2 \omega^2 R_T^2$$

giving

$$R_T \theta = \lambda^2 \omega^2 + \theta^2 \quad ,$$

$$R_T = \frac{\lambda^2 \omega^2}{\theta} + \theta,$$

and

$$C_T = \sqrt{\frac{R_T - \theta}{\theta}} \Big/ R_T\omega$$

$$= \sqrt{\frac{\frac{\lambda^2\omega^2}{\theta} + \theta - \theta}{\theta}} \Big/ R_T\omega$$

$$= \frac{\lambda}{R_T} = \frac{\lambda}{R_T} = \frac{\lambda\theta}{\lambda^2\omega^2 + \theta^2} \quad .$$